Nanoscale Advances

ROYAL SOCIETY OF CHEMISTRY

PAPER

View Article Online
View Journal | View Issue

Cite this: *Nanoscale Adv.*, 2020, **2**, 1685

A simple and straightforward strategy for synthesis of N,P co-doped porous carbon: an efficient support for Rh nanoparticles for dehydrogenation of ammonia borane and catalytic application†

Wenxiu Luo, Xue Zhao, Wei Cheng, Yun Zhang, Yi Wang * and Guangyin Fan *

Metal nanoparticles (NPs) deposited on nitrogen (N)- and/or phosphorus (P)-doped porous carbon have been investigated as efficient catalysts for hydrolysis of ammonia borane (AB). However, the one-pot synthesis of N,P co-doped porous carbon using low-cost and readily available sources is still a tremendous challenge. Herein, a novel one-pot methodology is developed to fabricate N and P co-doped porous carbon (ATP-C) using non-precious and easily available adenosine triphosphate (ATP). The process of N and P doping does not need additional N or P sources in the material. Moreover, the entire process did not require chemical activation agents, making it more practical for large-scale applications. The resulting ATP-C supported Rh NPs (Rh/ATP-C) exhibit excellent performance for the catalytic hydrolysis of ammonia borane toward hydrogen generation, with a total turnover frequency (TOF) value of 566 mol H_2 min^{-1} (mol Rh)$^{-1}$ and activation energy (E_a) of 26.3 kJ mol^{-1}. The catalytic system has shown an outstanding catalytic cycle life during the recycling tests. This work provides a novel method for the production of high performance carbon material supported metal NP catalysts for practical dehydrogenation applications.

Received 6th January 2020
Accepted 12th February 2020

DOI: 10.1039/d0na00007h

rsc.li/nanoscale-advances

1. Introduction

With the ever-increasing demands for energy consumption, new sustainable energy conversion and storage devices have become more and more important. Hydrogen (H_2) has been recognized as a potential clean energy carrier because of its high-energy density and clean burning nature.[1,2] However, the safe storage and efficient hydrogen release under ambient conditions are still a challenge.[3–5] As the simplest B–N based compound, ammonia borane (AB) has a high hydrogen content (19.6 wt%) with a low molecular weight (30.9 g mol^{-1}) and is stable under ambient conditions.[6,7] With suitable catalysts, 1 mole of ammonia borane can release 3 moles of hydrogen upon hydrolysis, as shown in eqn (1).[8,9]

$$NH_3BH_3(aq) + 2H_2O(l) \xrightarrow{\text{catalyst}} NH_4^+(aq) + BO_2^-(aq) + 3H_2(g) \quad (1)$$

Metal nanoparticles (MNPs), including noble metals (such as Rh, Ru, Pd, and Pt)[10–13] and non-noble metals (such as Fe, Co, Ni, and Cu),[14–17] have drawn much attention due to their excellent catalytic activity in AB hydrolysis. However, these metallic catalysts with the nanoscale size are liable to cause severe agglomeration, resulting in poor stability and efficiency, and even get inactivated in successive recycles. In response to this problem, deposition of different sizes of metal NPs on suitable supports for hydrolysis of AB has been proposed. The use of supports can disperse the MNPs well, and improved hydrogen-generation rates have been efficiently achieved. More importantly, supports can prevent MNP agglomeration and improve their stability and utilization, which is particularly crucial for noble metals considering their high-cost and scarcity. In recent years, various supports consisting of SiO_2,[18] γ-Al_2O_3,[19] carbon nanotubes (CNTs),[20] metal–organic frameworks (MOFs),[21] and porous carbon[22] have been used for hydrolysis of AB. In the exploration of these advanced supports, carbon materials have attracted considerable attention due to their high specific surface area and tunable porous structures.

On the other hand, doping with miscellaneous elements could adjust surface charge distribution and improve the energy storage/release performance. Porous carbon materials doped with heteroatoms (B, N, and P)[23–25] are more effective in catalytic performance. So far, the general method of N- or P-doping of carbon materials requires extra N or P sources (NH_3 and PH_3)[26] in the material preparation process or treatment of carbon materials with high concentration N compounds (urea)[27] or P-containing acids (H_3PO_4). The existing preparation processes

College of Chemistry and Materials Science, Sichuan Normal University, Chengdu 610068, P.R. China. E-mail: wangyi@sicnu.edu.cn; fanguangyin@sicnu.edu.cn

† Electronic supplementary information (ESI) available. See DOI: 10.1039/d0na00007h

are cumbersome and very dangerous to some degree. The straightforward access to N,P co-doped nanoporous carbon derived from available and common raw materials is rare. Therefore, the development of an economical, simple, and efficient method to obtain nanoporous carbon with multi-element doping (such as N and P) is a challenge, but it is in high demand.

We have reported that N or P-doped carbons as MNP supports enhanced catalytic activities for AB decomposition.[28–30] We have also been exploring a simple and effective method for N,P co-doped nanocarbon fabrication, which is promising from the viewpoints of both economical and environmental issues. In the choice of raw material enriched with N or P, adenosine triphosphate disodium (ATP) is an excellent candidate owing to the high abundance of N and P offered by one adenine structure and three phosphate groups, respectively. Furthermore, the presence of the strong anchoring groups of ATP with intrinsic N and P-coordination sites would facilitate the binding of metal ions. The formation of nucleation sites around ATP can confine the over-growth of Rh NPs and consequently control their particle size. Herein, we exploit an N,P co-doped carbon material derived from ATP for the first time and immobilize Rh NPs on the porous carbon toward the catalytic dehydrogenation of AB. The highly dispersed Rh NPs in the enriched N and P co-doped carbon exhibit excellent catalytic performance for hydrogen generation in the dehydrogenation of AB. The TOF of hydrolysis dehydrogenation of AB by the Rh/ATP-C-800 catalyst is 566 mol H_2 min^{-1} (mol Rh)$^{-1}$ at 25 ± 0.2 °C, which is higher than that of most reported Rh-based catalysts. These results demonstrate the validity of using N and P-rich complexes in constructing abundantly heteroatom co-doped porous carbon and efficient metal supports for the high performance in practical catalytic applications.

2. Experimental

2.1 Materials and chemicals

$RhCl_3 \cdot nH_2O$ (Rh content of 39 wt%) was purchased from Precious Metals Institute of Kunming, China. Adenosine triphosphate disodium ($C_{10}H_{14}N_5Na_2O_{13}P_3$, ATP-$Na_2$) was provided by Aladdin Reagent Company, Shanghai, China. Ammonia borane (AB, 90%) was purchased from Sigma-Aldrich. All chemicals were used without any purification. Deionized water was used in all experiments.

2.2 Preparation of porous carbon (ATP-C) derived from adenosine triphosphate disodium (ATP)

In a typical process, adenosine triphosphate disodium (3.0 g) was evenly put into two porcelain boats, which were subsequently placed in a quartz tube and heated at 800 °C for 2 h (heating rate of 5 °C min^{-1}) under an Ar atmosphere (flow rate of 30 mL min^{-1}). A gray-black solid was obtained and then ground into a powder in an agate mortar. After being washed with 1.0 M HCl and deionized water until the washing effluent reached a neutral pH of 7 at room temperature, the powder was dried at 60 °C for 10 h. The obtained carbon was named ATP-C-800. To further investigate the temperature effect of pyrolysis, the carbonization temperatures of the porous carbons for a similar treatment were selected to be 700 °C and 900 °C, respectively. The final porous carbons were denoted as ATP-C-700 and ATP-C-900, indicating the different carbonization temperatures.

2.3 Preparation of Rh(III)/ATP-C

In a typical synthesis, 50 mg of ATP-C was stirred in 20 mL methanol and dispersed for 20 min. After this, 7.4 mg $RhCl_3 \cdot nH_2O$ was added into the solution and the mixture was continually stirred in a water bath at a constant temperature of 60 ± 0.2 °C. The solution was evaporated and the black powder of Rh(III)/ATP-C with 5.8 wt% Rh loading was obtained finally. Furthermore, the corresponding powders of Rh(III)/ATP-C with 4.5 wt% Rh loading and 6.5 wt% Rh loading were synthesized to measure the trend of hydrolysis performance.

2.4 *In situ* formation of Rh/ATP-C and catalytic hydrolysis of AB by Rh/ATP-C

Specifically, 10 mg of Rh(III)/ATP-C was dispersed in 4 mL deionized water kept in a 25 mL two-neck flask. One neck of the flask was connected to a gas burette to measure the volume of hydrogen. After ultrasonicating for 20 min, the mixture was put in a magnetic stirrer keeping the temperature constant at 25 ± 0.2 °C. A solution of AB in 1.0 mL deionized water solution (containing 1.0 mmol of AB) was quickly injected into the reactor with a syringe. The catalytic hydrolysis of AB started immediately and Rh nanoparticles were supported on ATP-C, and the Rh/ATP-C catalyst was formed. For catalytic hydrolysis of AB by the Rh/ATP-C catalyst, after the first run of the hydrogen generation reaction was completed, the Rh/ATP-C catalyst was isolated from the reaction mixture and rinsed with water. The recovered black solid was transferred into the reactor and another 1.0 mmol of AB aqueous solution was subsequently added to the reaction system. The released gas was monitored using the gas burette and the reaction was completed when there was no more gas generation.

The reusability of the Rh/ATP-C catalyst was determined using the recovered catalyst after hydrolytic decomposition of AB. The recovered Rh catalyst from each cycle was washed three times with water and ethanol. When the fresh AB aqueous solution was introduced, the next recycling run was started. Recycling tests were repeated eight times.

2.5 UV-vis absorption spectrum measurements of 4-nitrophenol

The UV-vis absorption spectra of 4-nitrophenol (4-NPh) in the presence of AB were monitored over the wavelength range from 250 to 500 nm. The process was carried out in a well-stoppered quartz cuvette. In a typical process, 0.2 mL of the Rh/ATP-C catalyst dispersion (0.2 mg mL^{-1}) was added to 2.0 mL of 4-NPh stock solution (0.0625 mM). Then 1.0 mL of freshly prepared AB aqueous solution (contain 1 mmol AB) was added to the above solution and UV-visible absorption spectra were monitored at different time intervals.

2.6 Characterization

Powder X-ray diffraction (XRD) measurements were carried out using a Rigaku Ultima IV diffractometer with Cu Kα radiation. Scanning electron microscopy (SEM) images were obtained using a JEOL JSM-5310LV at 15 kV and 33 Pa in a low-vacuum mode without metal coating on the aluminum support. The morphologies of all the samples were observed using a transmission electron microscope (TEM, JEM-2010). The X-ray photoelectron spectra (XPS) were acquired with an ESCALAB250 (Thermo VG Corp). FT-IR spectra were collected at room temperature by using a Thermo FTIR-iS10 instrument using KBr discs in the 400–4000 cm^{-1} region. The surface area of the samples is calculated by the Brunauer–Emmet–Teller (BET) method.

3. Results and discussion

As illustrated in Scheme 1, ATP-C was synthesized from ATP by a one-step heat treatment process. In addition to the carbon source, ATP is also used as the N and P sources owing to its high N (12.71%) and P (16.86%) contents. After the high-temperature carbonization and being leached with 1.0 M HCl, the black carbonaceous carbon product ATP-C was obtained. In the process, the N and P co-doped porous carbon derived from a low-cost material was formed. Most importantly, the process for N and P-doping did not require additional N or P sources (NH_3 and PH_3) in the material or treatment of carbon materials with strong bases, making its large-scale use more practical. Then, a small quantity of $RhCl_3 \cdot nH_2O$ was added to the above-mentioned ATP-C sample and Rh^{3+} can be uniformly coated on the carbon due to the interaction between negative N, O and P groups and Rh(III) cations. After the addition of AB into the solution, the black Rh/ATP-C catalyst was finally produced and the catalytic hydrolysis of AB started at the same time.

To understand the effect of temperature on the specific surface area and porosity of ATP-C, N_2 adsorption–desorption analysis was performed (Fig. 1a). The BET surface areas of the as-prepared ATP-C-700, ATP-C-800 and ATP-C-900 were 118.7 $m^2 g^{-1}$, 154.2 $m^2 g^{-1}$ and 51.2 $m^2 g^{-1}$, respectively, all of which were small and decrease sharply at carbonization temperature higher than 800 °C. It is worthy to mention that the average pore diameter of ATP-C-800 (6.83 nm) was larger than that of ATP-C-700 (3.96 nm) and ATP-C-900 (3.89 nm), confirming the pore forming effect of temperature (Fig. 1a and S1†). Based on the above results, 800 °C was considered to be the optimal carbonization temperature. The FT-IR spectra of ATP-C-800 and Rh/ATP-C-800 proved the existence of O-, N- and P-containing groups on the surface of the samples (Fig. 1c). The broad absorption peak in a range of 3269–3335 cm^{-1} was assigned to the stretching vibrations of N–H and the characteristic peaks at 2882–2958 cm^{-1} correspond to $-CH_2$. The peaks at 1626 cm^{-1} and 1050 cm^{-1} can be attributed to the vibration frequencies of the C=O group and C–O group, respectively. It is worthy to note that the stretching peak at 1440 cm^{-1} corresponds to the C–P bond,[31] which was well consistent with the elemental mappings and XPS results of Rh/ATP-C-800. The microstructure variations of ATP-C-800 and Rh/ATP-C-800 were characterized by XRD (Fig. 1d). The two weak broad diffraction peaks at 24° and 43° in the XRD patterns indicate that the ATP-C-800 was an amorphous carbon containing a highly disordered structure. No obvious diffraction peaks about Rh species were observed, which might be due to low Rh NP loading and the traps of ultrafine Rh NPs in the pores of ATP-C-800.

The scanning electron microscopy (SEM) image shows the morphology of ATP-C-800 resembling an irregular sheet structure (Fig. 2a). The energy-dispersive X-ray spectroscopy (EDX) mapping analysis of ATP-C-800 proves the coexistence and homogeneous dispersion of N, O, and P elements (Fig. 2b). Besides, the weight ratios of O, N and P elements on the surface of the carbon framework were about 14.82%, 2.54% and 0.3%.

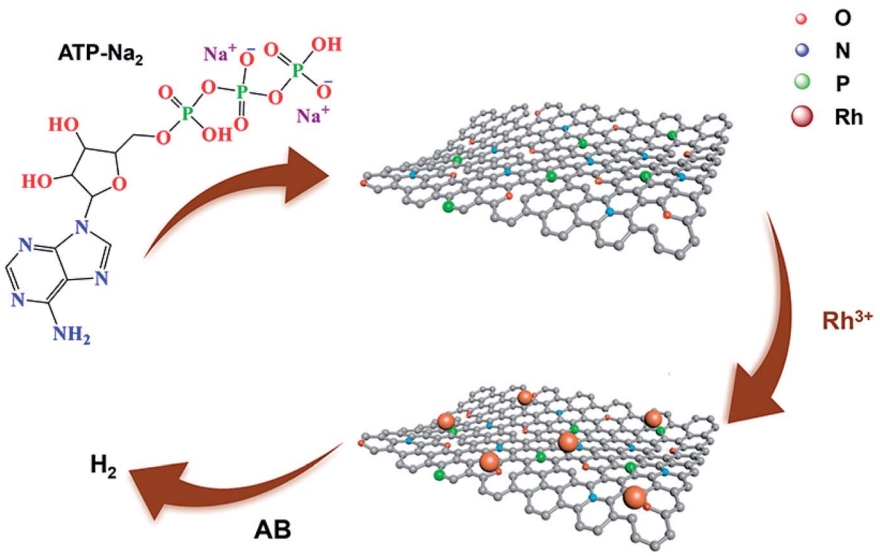

Scheme 1 Schematic illustration of the synthesis process of Rh/ATP-C.

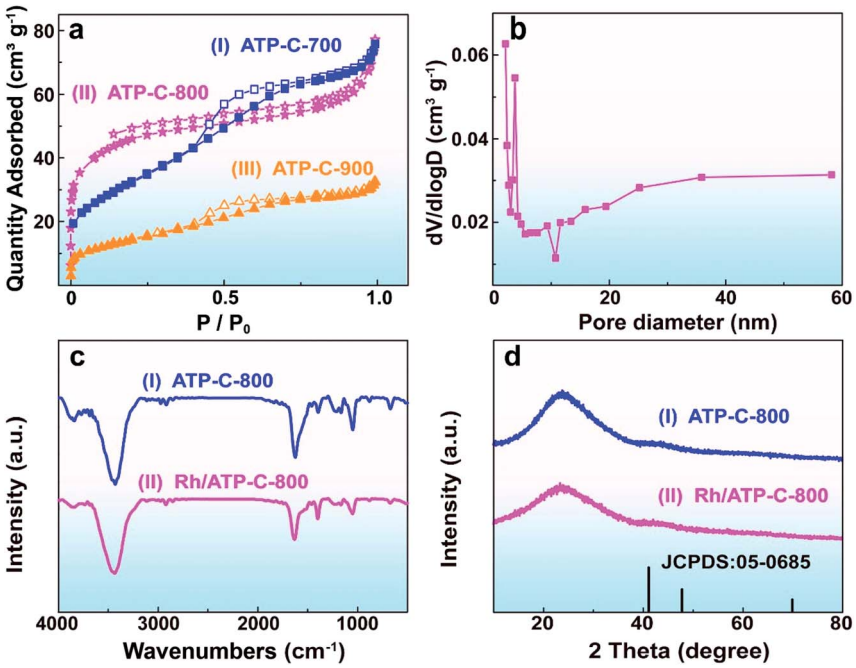

Fig. 1 (a) The BET spectra of ATP-C-700, ATP-C-800 and ATP-C-900. (b) The pore size distribution of ATP-C-800. (c) The FT-IR spectra of ATP-C-800 and Rh/ATP-C-800. (d) The XRD patterns of ATP-C-800 and Rh/ATP-C-800.

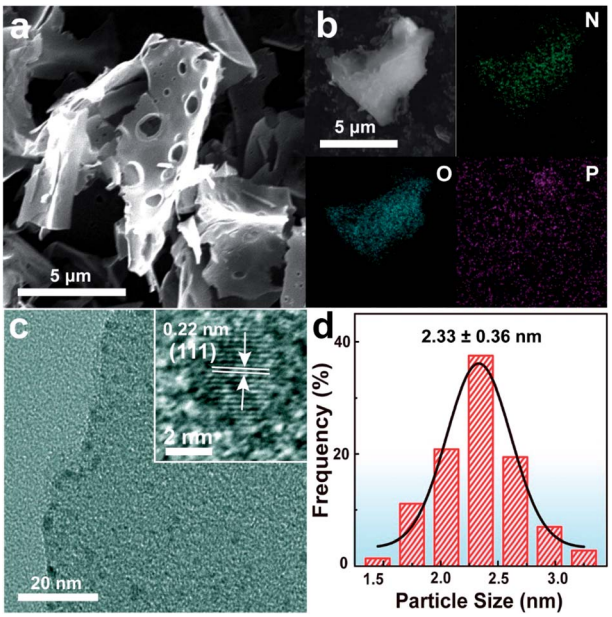

Fig. 2 (a) The SEM image of ATP-C-800. (b) The C, N, O, and P elemental mappings of ATP-C-800. (c) The TEM image of Rh/ATP-C-800 (inset shows the HRTEM image of Rh/ATP-C-800). (d) The particle size distribution of Rh/ATP-C-800 with 5.8 wt% Rh loading.

The acid cleaning in the synthesis process might result in the loss of phosphate to some extent. On the other hand, the higher N content might be related to its stable forms of graphitic/pyridine/pyrrole nitrogen. However, P-doping occurs with the bonding configuration of C–P/O–P. The lower content of P is similar to the other N, P and S co-doped carbon.[32–34] After loading the Rh NPs, the transmission electron microscopy (TEM) image of the ATP-C-800 sample was flaky, and the metal nanoparticles were obviously deposited on the surface of the carbon nanosheets (Fig. 2c). A lattice fringe of 0.22 nm could be obtained in the high-magnification TEM images of the Rh/ATP-C-800 catalyst. The dark spots of Rh nanoparticles were found to be well dispersed with an average particle diameter of 2.33 ± 0.36 nm by performing particle size statistics (Fig. 2d).

The X-ray photoelectron spectroscopy (XPS) analysis was conducted to determine the elements of the catalyst and their corresponding chemical states. The full scan spectrum of Rh/ATP-C-800 distinctly revealed the presence of C, N, O, and P, which was in good agreement with the EDX mapping analysis. High-resolution XPS spectra of the detected elements were recorded accordingly. The binding energies of 314 and 309.3 eV were attributed to Rh(III) of Rh $3d_{3/2}$ and Rh $3d_{5/2}$, while the characteristic peaks of Rh(0) of $3d_{3/2}$ and $3d_{5/2}$ appeared at 312.3 and 307.6 eV (Fig. 3b).[35] The detectable Rh(III) species can be ascribed to the surface Rh combined with oxygen in the atmosphere during the catalyst preparation and storage process, which is similar to the other Rh-based catalysts.[36,37] Owing to the presence of oxygen-containing groups observed from the spectra of O 1s and C 1s, it is very hard to quantitatively determine the Rh to O molar ratio. Therefore, the resulting Rh(III) species of Rh/ATP-C-800 was denoted as RhO_x. Due to the N and P influence on the surface electrons of the Rh/ATP-C-800 catalyst, a value of 0.4 eV was derived from the theoretical values (311.9 and 307.2 eV). The peaks of C 1s were at 284.5, 285.2, 286.2, and 287.6 eV, corresponding to the sp2 carbon, C–N, C–P and C–O, respectively (Fig. 3c). The peaks of N 1s at 400.6, 399.4 and 398.5 eV were assigned to graphitic N,

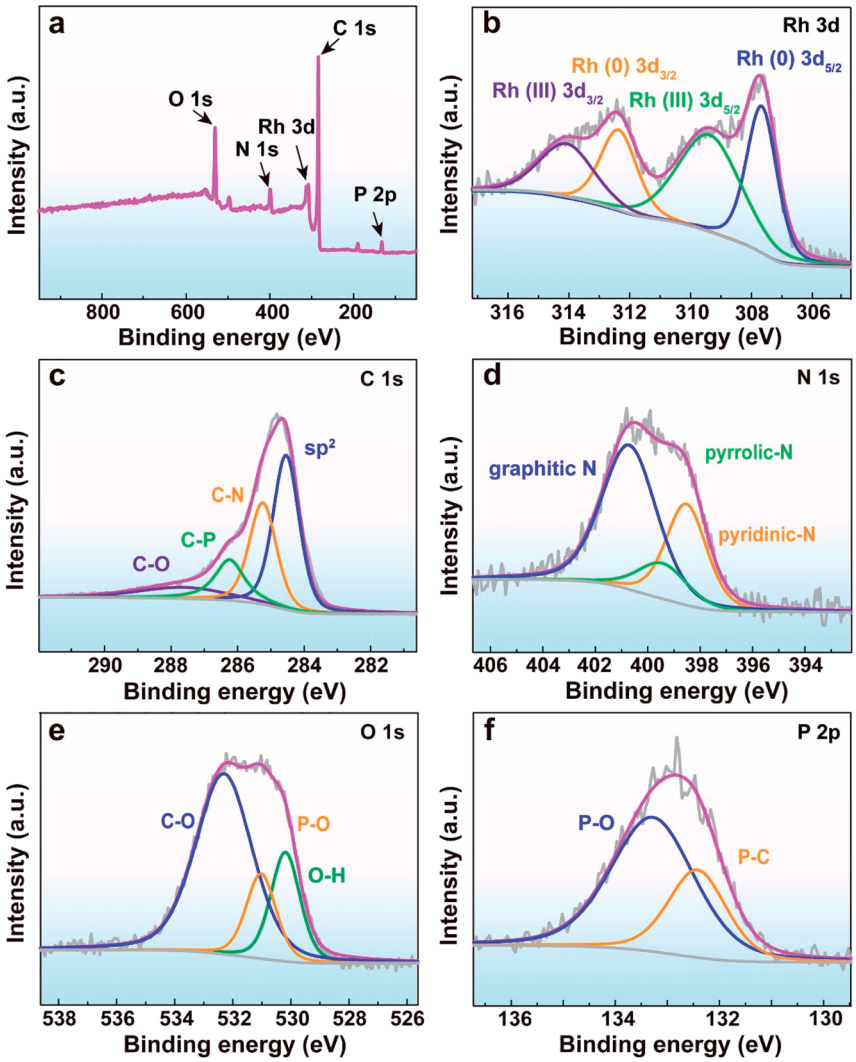

Fig. 3 (a) The XPS spectrum of the Rh/ATP-C-800 catalyst. (b–f) The high-resolution spectra: (b) Rh 3d, (c) C 1s, (d) N 1s, (e) O 1s, and (f) P 2p, respectively.

pyrrolic N, and pyridinic N, respectively (Fig. 3d).[38] The three peaks of O 1s at C–O, P–O and O–H correspond to 532.3, 531 and 530.2 eV (Fig. 3e). The two peaks of P 2p at 133.3 and 132.4 eV could be attributed to the P–O bond and the P–C bond, respectively (Fig. 3f).[39]

To shed light on the role of ATP-C-800 as the efficient support in improving the catalytic performance, we studied the rate of hydrogen evolution of AB hydrolysis with the ATP-C-800, Rh NPs, Rh/XC-72R and Rh/ATP-C-800 as catalysts, respectively (Fig. S3†). In the absence of Rh NPs, the ATP-C-800 did not catalyze AB dehydrogenation. The Rh NP catalyst without any supports had a low dehydrogenation capability of 54 mol H_2 min^{-1} (mol Rh)$^{-1}$, primarily due to the aggregation of the Rh NPs during the catalysis of AB. The Rh NPs supported on carbon black (Rh/XC-72R) without nitrogen and phosphorus showed catalytic activity with a TOF of 167 mol H_2 min^{-1} (mol Rh)$^{-1}$. When Rh NPs were deposited on ATP-C-800, the same Rh loading (5.8 wt%) provided an efficient performance for hydrogen release, giving the initial turnover frequency of 566 mol H_2 min^{-1} (mol Rh)$^{-1}$. It has been reported that heteroatom-doped carbon materials would change the catalytic performance of the catalyst due to the interconnectedness of the surface metal atoms and heteroatoms, increasing the dehydrogenation rate.[40] Thus, we presumed that the contribution of ATP-C enriched with N and P-atoms not only dispersed the Rh NPs and inhibited the metal NP aggregation, but also endowed Rh NPs with more accessible surface active sites.

The effects of the Rh concentration, the amount of AB and the reaction temperature on the AB dehydrogenation rate were measured to interpret the kinetics of AB hydrolysis. When the Rh concentration was 1.13 mM, a TOF value of 566 mol H_2 min^{-1} (mol Rh)$^{-1}$ was obtained, which was higher than most of the reported results (Table S1†).[10,20,37,41–43] A good linear relationship was observed between the ln rate and the ln[Rh]. The hydrolysis follows first-order kinetics with respect to the Rh concentration (Fig. 4b). The logarithmic plots of the hydrogen generation rate *versus* AB concentration are shown in Fig. 4a

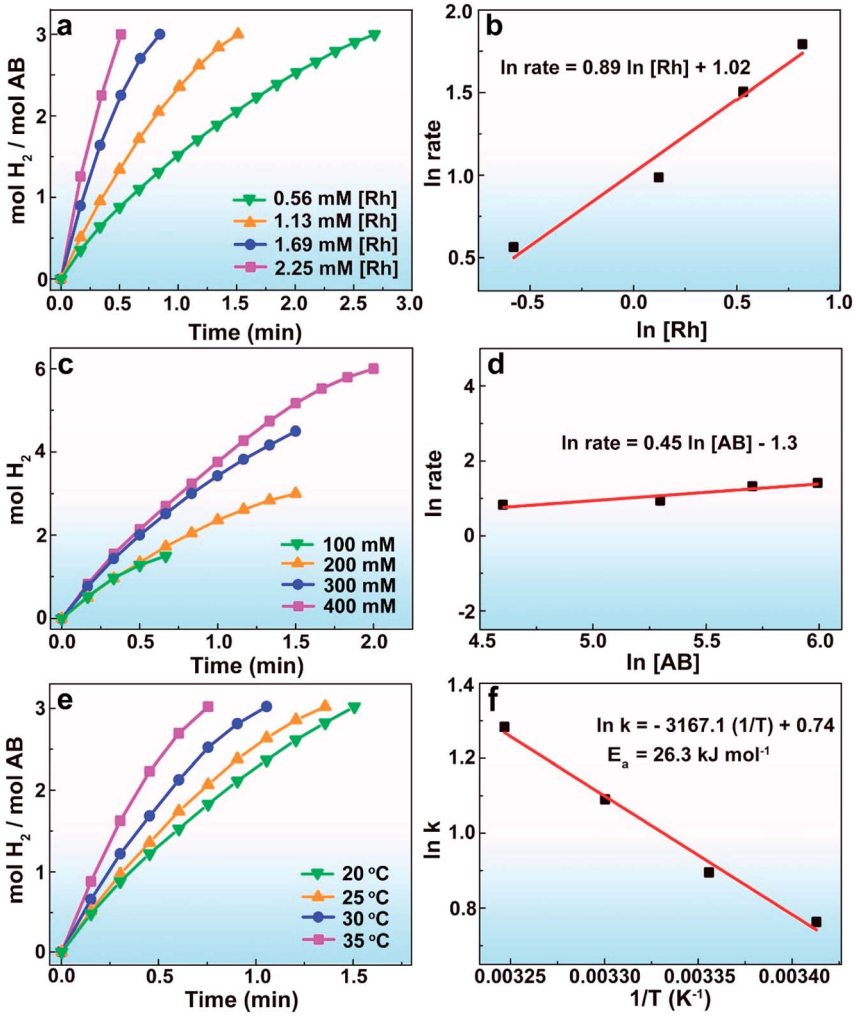

Fig. 4 Time course plot of H_2 generation for the hydrolysis of AB over Rh/ATP-C-800, (a) with different Rh concentrations, (b) the logarithmic plot of the hydrogen generation rate *versus* the Rh concentration, (c) with different AB concentrations, (d) the logarithmic plot of the hydrogen generation rate *versus* the AB concentration, (e) at different temperatures, and (f) the Arrhenius plot (ln *k versus* 1/*T*).

and b, where the line slope was calculated to be 0.45, suggesting that the dehydrogenation of AB by Rh/ATP-C-800 was zero order in terms of the AB concentration.[44] When the reaction temperature was increased, the hydrogen generation rate increased, indicating that the hydrolysis temperature had a positive effect on the catalyst activity. The Arrhenius equation (2) was used to calculate the activation energy (E_a) of the Rh/ATP-C catalyst for the dehydrogenation of AB.[45]

$$\ln K = \ln A - \frac{E_a}{RT} \quad (2)$$

An activation energy of 26.3 kJ mol^{-1} was obtained from the plot of ln *k versus* 1/*T*, which was lower than most of the reported values.[10,20,37,41–43] The lower activation energy indicated the excellent catalytic performance of the as-synthesized Rh/ATP-C-800.

The recyclability and stability of catalysts play a key role in practical applications. After completion of hydrolysis of AB, the Rh/ATP-C-800 catalyst was isolated from the reaction mixture. The recovered catalyst was rinsed with water, transferred into a reactor, and rapidly injected with another equivalent of AB to start the next recycling. The Rh/ATP-C-800 catalyst still retains 63% of its initial catalytic activity after the eighth catalytic run, indicating that the Rh/ATP-C-800 catalyst has good potential for practical applications (Fig. 5a and b). After recycling tests, the catalyst was filtered, and the morphology and size of the recycled catalyst were investigated by XRD and TEM analysis. The XRD pattern indicated that there was no significant structural change of Rh/ATP-C-800 during the recycle tests, but the TEM image indicated that some of the MNPs had been agglomerated after the eighth test (Fig. S4 and S5†). The agglomeration of the MNP catalyst after eight runs could be due to the increased viscosity of the solution mixture during the hydrolysis of AB. Furthermore, the XPS spectrum showed that there was no discernible change of the valence state of Rh species during the hydrolysis reaction (Fig. S6†). Therefore, the decrease of catalytic activity could be due to the agglomeration of some Rh NPs and the loss of a small amount of catalyst in the course of the test carried out many times.

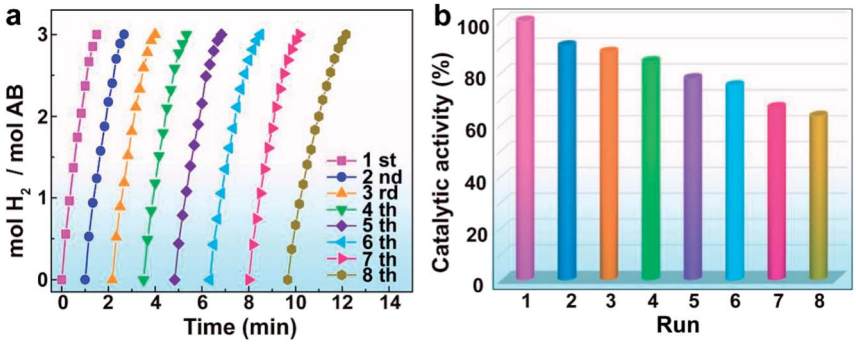

Fig. 5 (a) Hydrogen generation from AB catalyzed by Rh/ATP-C-800 from the first to eighth cycles. (b) Percentage of the initial catalytic activity of Rh/ATP-C-800 in eight successive runs at room temperature.

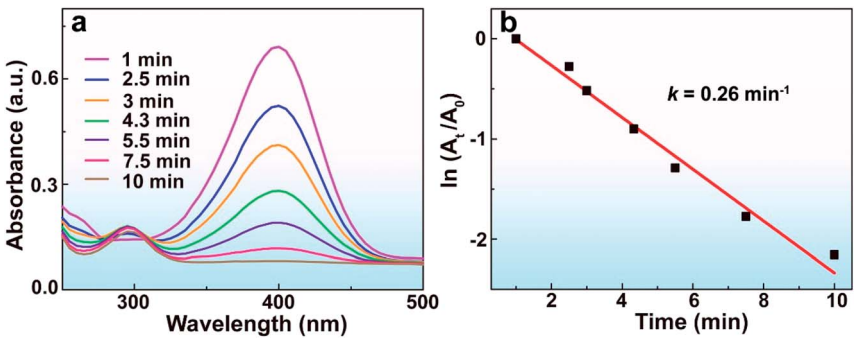

Fig. 6 (a) UV-vis spectra of gradual reduction of 4-NPh catalyzed by Rh/ATP-C-800 at room temperature. (b) The corresponding slope of the plot $\ln(A_t/A_0)$ *vs.* reaction time (min).

It is worth mentioning that the Rh/ATP-C-800 catalyst could be applied to other catalytic reactions. We evaluated the catalytic performance of Rh/ATP-C-800 in the reduction of 4-NPh. The characteristic absorbance of 4-NPh at $\lambda = 400$ nm could be readily monitored by UV-vis spectroscopy. After the reaction period of time, a new characteristic peak appeared at $\lambda = 295$ nm. In the presence of Rh/ATP-C-800 (0.04 mg) and AB (1 mmol), 4-NPh (0.125 M) was completely reduced within 10 minutes (Fig. 6a). The linear relationship between $\ln(A_t/A_0)$ and t (min) is shown in Fig. 6b, representing the absorbance at the intervals and the initial stage of 4-nitrophenolate ions. The pseudo-first-order rate constant (k) is estimated to be 0.26 min^{-1}, which was superior to that of Rh-based catalysts under ambient conditions.[46,47] Such a catalytic activity further demonstrates the potential application of this catalyst in the catalytic field.

4. Conclusions

In summary, a facile and straightforward heat-treatment strategy to prepare N,P-functionalized porous carbon materials derived from available ATP has been developed. In addition to carbon sources, ATP was used as the N and P sources owing to its high nitrogen and phosphorus contents. The ATP-C with self-doped N- and P-group immobilized Rh NPs (Rh/ATP-C) exhibited an unexpected talent for catalytic dehydrogenation of AB hydrolysis and provided excellent stability and recyclability in the catalytic reaction. Such an enhanced catalytic activity was demonstrated toward the 4-NPh reduction reaction and showed superior catalytic performance, illustrating the potential applications of the catalyst. This work may offer a new method for the exploration of advanced carbon supported catalysts, combining the advantages of both a feasible strategy and promising practical applications.

Conflicts of interest

There are no conflicts to declare.

Acknowledgements

This work was financially supported by the Natural Science Foundation of Sichuan Provincial Department of Education (17ZA0330), the Opening Project of Key Laboratory of Green Chemistry of Sichuan Institutes of Higher Education (LZJ1603), and the National Natural Science Foundation of China (21777109).

References

1 A. Zuttel, A. Remhof, A. Borgschulte and O. Friedrichs, Hydrogen: the future energy carrier, *Philos. Trans. R. Soc., A*, 2010, **368**(1923), 3329–3342.

2 A. Bulut, M. Yurderi, İ. E. Ertas, M. Celebi, M. Kaya and M. Zahmakiran, Carbon dispersed copper-cobalt alloy nanoparticles: A cost-effective heterogeneous catalyst with exceptional performance in the hydrolytic dehydrogenation of ammonia-borane, *Appl. Catal., B*, 2016, **180**, 121–129.

3 L. Guo, X. Gu, K. Kang, Y. Wu, J. Cheng, P. Liu, T. Wang and H. Su, Porous nitrogen-doped carbon-immobilized bimetallic nanoparticles as highly efficient catalysts for hydrogen generation from hydrolysis of ammonia borane, *J. Mater. Chem. A*, 2015, **3**(45), 22807–22815.

4 J. Cheng, X. Gu, P. Liu, T. Wang and H. Su, Controlling catalytic dehydrogenation of formic acid over low-cost transition metal-substituted AuPd nanoparticles immobilized by functionalized metal–organic frameworks at room temperature, *J. Mater. Chem. A*, 2016, **4**(42), 16645–16652.

5 Q. Wang, T. Hisatomi, Q. Jia, H. Tokudome, M. Zhong, C. Wang, Z. Pan, T. Takata, M. Nakabayashi, N. Shibata, Y. Li, I. D. Sharp, A. Kudo, T. Yamada and K. Domen, Scalable water splitting on particulate photocatalyst sheets with a solar-to-hydrogen energy conversion efficiency exceeding 1%, *Nat. Mater.*, 2016, **15**, 611.

6 X. Du, C. Yang, X. Zeng, T. Wu, Y. Zhou, P. Cai, G. Cheng and W. Luo, Amorphous NiP supported on rGO for superior hydrogen generation from hydrolysis of ammonia borane, *Int. J. Hydrogen Energy*, 2017, **42**(20), 14181–14187.

7 Z. Li, T. He, L. Liu, W. Chen, M. Zhang, G. Wu and P. Chen, Covalent triazine framework supported non-noble metal nanoparticles with superior activity for catalytic hydrolysis of ammonia borane: from mechanistic study to catalyst design, *Chem. Sci.*, 2017, **8**(1), 781–788.

8 W.-W. Zhan, Q.-L. Zhu and Q. Xu, Dehydrogenation of Ammonia Borane by Metal Nanoparticle Catalysts, *ACS Catal.*, 2016, **6**(10), 6892–6905.

9 Q. Yao, K. Yang, X. Hong, X. Chen and Z.-H. Lu, Base-promoted hydrolytic dehydrogenation of ammonia borane catalyzed by noble-metal-free nanoparticles, *Catal. Sci. Technol.*, 2018, **8**(3), 870–877.

10 J. Shen, L. Yang, K. Hu, W. Luo and G. Cheng, Rh nanoparticles supported on graphene as efficient catalyst for hydrolytic dehydrogenation of amine boranes for chemical hydrogen storage, *Int. J. Hydrogen Energy*, 2015, **40**(2), 1062–1070.

11 S. Akbayrak, Y. Tonbul and S. Ozkar, Ceria-supported ruthenium nanoparticles as highly active and long-lived catalysts in hydrogen generation from the hydrolysis of ammonia borane, *Dalton Trans.*, 2016, **45**(27), 10969–10978.

12 Y. Tonbul, S. Akbayrak and S. Özkar, Palladium(0) nanoparticles supported on ceria: highly active and reusable catalyst in hydrogen generation from the hydrolysis of ammonia borane, *Int. J. Hydrogen Energy*, 2016, **41**(26), 11154–11162.

13 J. K. Sun, Z. Kochovski, W. Y. Zhang, H. Kirmse, Y. Lu, M. Antonietti and J. Yuan, General Synthetic Route toward Highly Dispersed Metal Clusters Enabled by Poly(ionic liquid)s, *J. Am. Chem. Soc.*, 2017, **139**(26), 8971–8976.

14 G. Srinivas, W. Travis, J. Ford, H. Wu, Z.-X. Guo and T. Yildirim, Nanoconfined ammonia borane in a flexible metal–organic framework Fe–MIL-53: clean hydrogen release with fast kinetics, *J. Mater. Chem. A*, 2013, **1**(13), 4167.

15 C. Tang, F. Qu, A. M. Asiri, Y. Luo and X. Sun, CoP nanoarray: a robust non-noble-metal hydrogen-generating catalyst toward effective hydrolysis of ammonia borane, *Inorg. Chem. Front.*, 2017, **4**(4), 659–662.

16 J. Zhang, C. Chen, W. Yan, F. Duan, B. Zhang, Z. Gao and Y. Qin, Ni nanoparticles supported on CNTs with excellent activity produced by atomic layer deposition for hydrogen generation from the hydrolysis of ammonia borane, *Catal. Sci. Technol.*, 2016, **6**(7), 2112–2119.

17 Y. W. Yang, Z. H. Lu and X. S. Chen, Cu-based nanocatalysts for hydrogen generation via hydrolysis and methanolysis of ammonia borane, *Mater. Technol.*, 2015, **30**(sup2), A89–A93.

18 Q. Yao, W. Shi, G. Feng, Z.-H. Lu, X. Zhang, D. Tao, D. Kong and X. Chen, Ultrafine Ru nanoparticles embedded in SiO_2 nanospheres: Highly efficient catalysts for hydrolytic dehydrogenation of ammonia borane, *J. Power Sources*, 2014, **257**, 293–299.

19 G. P. Rachiero, U. B. Demirci and P. Miele, Bimetallic RuCo and RuCu catalysts supported on γ-Al_2O_3. A comparative study of their activity in hydrolysis of ammonia-borane, *Int. J. Hydrogen Energy*, 2011, **36**(12), 7051–7065.

20 Q. Yao, Z.-H. Lu, Y. Jia, X. Chen and X. Liu, In situ facile synthesis of Rh nanoparticles supported on carbon nanotubes as highly active catalysts for H2 generation from NH3BH3 hydrolysis, *Int. J. Hydrogen Energy*, 2015, **40**(5), 2207–2215.

21 C. Wang, J. Tuninetti, Z. Wang, C. Zhang, R. Ciganda, L. Salmon, S. Moya, J. Ruiz and D. Astruc, Hydrolysis of Ammonia-Borane over Ni/ZIF-8 Nanocatalyst: High Efficiency, Mechanism, and Controlled Hydrogen Release, *J. Am. Chem. Soc.*, 2017, **139**(33), 11610–11615.

22 L. Zhou, J. Meng, P. Li, Z. Tao, L. Mai and J. Chen, Ultrasmall cobalt nanoparticles supported on nitrogen-doped porous carbon nanowires for hydrogen evolution from ammonia borane, *Mater. Horiz.*, 2017, **4**(2), 268–273.

23 Y. Men, J. Su, X. Du, L. Liang, G. Cheng and W. Luo, CoBP nanoparticles supported on three-dimensional nitrogen-doped graphene hydrogel and their superior catalysis for hydrogen generation from hydrolysis of ammonia borane, *J. Alloys Compd.*, 2018, **735**, 1271–1276.

24 F. Zhang, C. Ma, Y. Zhang, H. Li, D. Fu, X. Du and X.-M. Zhang, N-doped mesoporous carbon embedded Co nanoparticles for highly efficient and stable H_2 generation from hydrolysis of ammonia borane, *J. Power Sources*, 2018, **399**, 89–97.

25 C.-C. Hou, Q. Li, C.-J. Wang, C.-Y. Peng, Q.-Q. Chen, H.-F. Ye, W.-F. Fu, C.-M. Che, N. López and Y. Chen, Ternary Ni–Co–P nanoparticles as noble-metal-free catalysts to boost the hydrolytic dehydrogenation of ammonia-borane, *Energy Environ. Sci.*, 2017, **10**(8), 1770–1776.

26 L. S. Panchakarla, K. S. Subrahmanyam, S. K. Saha, A. Govindaraj, H. R. Krishnamurthy, U. V. Waghmare and C. N. R. Rao, Synthesis, Structure, and Properties of Boron-

and Nitrogen-Doped Graphene, *Adv. Mater.*, 2009, **21**(46), 4726–4730.

27 H.-L. Guo, P. Su, X. Kang and S.-K. Ning, Synthesis and characterization of nitrogen-doped graphene hydrogels by hydrothermal route with urea as reducing-doping agents, *J. Mater. Chem. A*, 2013, **1**(6), 2248–2255.

28 R. Lu, C. Xu, Q. Wang, Y. Wang, Y. Zhang, D. Gao, J. Bi and G. Fan, Ruthenium nanoclusters distributed on phosphorus-doped carbon derived from hypercrosslinked polymer networks for highly efficient hydrolysis of ammonia-borane, *Int. J. Hydrogen Energy*, 2018, **43**(39), 18253–18260.

29 C. Xu, M. Hu, Q. Wang, G. Fan, Y. Wang, Y. Zhang, D. Gao and J. Bi, Hyper-cross-linked polymer supported rhodium: an effective catalyst for hydrogen evolution from ammonia borane, *Dalton Trans.*, 2018, **47**(8), 2561–2567.

30 F. Zhong, Q. Wang, C. Xu, Y. Yang, Y. Wang, Y. Zhang, D. Gao, J. Bi and G. Fan, Ultrafine and highly dispersed Ru nanoparticles supported on nitrogen-doped carbon nanosheets: efficient catalysts for ammonia borane hydrolysis, *Appl. Surf. Sci.*, 2018, **455**, 326–332.

31 W. He, F. Zhang and H. Li, Active and reusable Pd(II) organometallic catalyst covalently bonded to mesoporous silica nanospheres for water-medium organic reactions, *Chem. Sci.*, 2011, **2**(5), 961–966.

32 K. Chen, Y. Hao, M. Zhang, D. Zhou, Y. Cao, Y. Wang and L. Feng, Nitrogen, sulfur and phosphorus-codoped carbon with a tunable nanostructure as an efficient electrocatalyst for the oxygen reduction reaction, *RSC Adv.*, 2017, **7**(10), 5782–5789.

33 H. Meng, X. Chen, T. Gong, H. Liu, Y. Liu, H. Li and Y. Zhang, N, P, S/Fe-codoped Carbon Derived from Feculae Bombycis as an Efficient Electrocatalyst for Oxygen Reduction Reaction, *ChemCatChem*, 2019, **11**(24), 6015–6021.

34 W. Wan, Q. Wang, L. Zhang, H.-W. Liang, P. Chen and S.-H. Yu, N-, P- and Fe-tridoped nanoporous carbon derived from plant biomass: an excellent oxygen reduction electrocatalyst for zinc–air batteries, *J. Mater. Chem. A*, 2016, **4**(22), 8602–8609.

35 D. Özhava and S. Özkar, Nanoalumina-supported rhodium(0) nanoparticles as catalyst in hydrogen generation from the methanolysis of ammonia borane, *Mol. Catal.*, 2017, **439**, 50–59.

36 W. Luo, W. Cheng, M. Hu, Q. Wang, X. Cheng, Y. Zhang, Y. Wang, D. Gao, J. Bi and G. Fan, Ultrahigh Catalytic Activity of l-Proline-Functionalized Rh Nanoparticles for Methanolysis of Ammonia Borane, *ChemSusChem*, 2019, **12**(2), 535–541.

37 M. Hu, M. Ming, C. Xu, Y. Wang, Y. Zhang, D. Gao, J. Bi and G. Fan, Towards High-Efficiency Hydrogen Production through in situ Formation of Well-Dispersed Rhodium Nanoclusters, *ChemSusChem*, 2018, **11**(18), 3253–3258.

38 X. Chen, J. Zheng, X. Zhong, Y. Jin, G. Zhuang, X. Li, S. Deng and J.-g. Wang, Tuning the confinement space of N-carbon shell-coated ruthenium nanoparticles: highly efficient electrocatalysts for hydrogen evolution reaction, *Catal. Sci. Technol.*, 2017, **7**(21), 4964–4970.

39 C. Li, S. Dong, R. Tang, X. Ge, Z. Zhang, C. Wang, Y. Lu and L. Yin, Heteroatomic interface engineering in MOF-derived carbon heterostructures with built-in electric-field effects for high performance Al-ion batteries, *Energy Environ. Sci.*, 2018, **11**(11), 3201–3211.

40 W. Ai, W. Zhou, Z. Du, Y. Chen, Z. Sun, C. Wu, C. Zou, C. Li, W. Huang and T. Yu, Nitrogen and phosphorus codoped hierarchically porous carbon as an efficient sulfur host for Li-S batteries, *Energy Storage Materials*, 2017, **6**, 112–118.

41 S. Akbayrak, Y. Tonbul and S. Özkar, Ceria supported rhodium nanoparticles: Superb catalytic activity in hydrogen generation from the hydrolysis of ammonia borane, *Appl. Catal., B*, 2016, **198**, 162–170.

42 Y. Tonbul, S. Akbayrak and S. Özkar, Group 4 oxides supported Rhodium(0) catalysts in hydrolytic dehydrogenation of ammonia borane, *Int. J. Hydrogen Energy*, 2019, **44**(27), 14164–14174.

43 J. Chen, M. Hu, M. Ming, C. Xu, Y. Wang, Y. Zhang, J. Wu, D. Gao, J. Bi and G. Fan, Carbon-supported small Rh nanoparticles prepared with sodium citrate: toward high catalytic activity for hydrogen evolution from ammonia borane hydrolysis, *Int. J. Hydrogen Energy*, 2018, **43**(5), 2718–2725.

44 H. Jia, X.-J. Liu, X. Chen, X.-X. Guan, X.-C. Zheng and P. Liu, Chitosan–Fe_3O_4 anchored palladium nanoparticles: An efficiently magnetic catalyst for hydrolytic dehydrogenation of ammonia borane, *Int. J. Hydrogen Energy*, 2017, **42**(47), 28425–28433.

45 K. Mori, K. Miyawaki and H. Yamashita, Ru and Ru–Ni Nanoparticles on TiO_2 Support as Extremely Active Catalysts for Hydrogen Production from Ammonia–Borane, *ACS Catal.*, 2016, **6**(5), 3128–3135.

46 S. Kundu, K. Wang and H. Liang, Photochemical Generation of Catalytically Active Shape Selective Rhodium Nanocubes, *J. Phys. Chem. C*, 2009, **113**(43), 18570–18577.

47 N. Moitra, K. Kanamori, Y. H. Ikuhara, X. Gao, Y. Zhu, G. Hasegawa, K. Takeda, T. Shimada and K. Nakanishi, Reduction on reactive pore surfaces as a versatile approach to synthesize monolith-supported metal alloy nanoparticles and their catalytic applications, *J. Mater. Chem. A*, 2014, **2**(31), 12535.